Observation of the chemiluminescent NO + O → NO_2 + *hν* reaction in the upper mesospheric dark polar regions by OSIRIS on Odin

R.L. Gattinger, W.F.J. Evans, ~~Ian~~ McDade, D.A. Degenstein, and E.J. Llewellyn

Abstract: The visible and near infrared continuum spectrum produced by the NO + O → NO_2 + *hν* chemiluminescent reaction has been detected in the upper mesospheric dark polar regions by OSIRIS on the Odin spacecraft. Averaged observed NO_2 emission spectral shapes are obtained by spectrally resolving the NO + O continuum from the blended strong upper mesospheric OH vibration–rotation airglow bands. The observed continuum spectral shape when compared with laboratory measurements is shifted to lower wavelengths by approximately 20 nm in the steeply sloped 400 to 500 nm region. The observed laboratory continuum spectral shape for upper mesospheric ambient pressure is presented for reference over the 400 to 800 nm region. An example of an NO_2 continuum volume emission-rate altitude profile derived from a single OSIRIS limb scan is also included. Limb radiances up to 3×10^9 photons cm^{-2} nm^{-1} s^{-1} are observed at the peak of the NO_2 continuum corresponding to total volume emission rates of approximately 2×10^4 photons cm^{-3} s^{-1}. Data extracted from numerous single-volume emission-rate altitude profiles obtained over approximately a 24 h period are assembled into a Southern Hemisphere polar map of the 90 km NO_2 continuum emission. The map illustrates the considerable spatial brightness variation typically observed in the dark Antarctic polar region throughout the OSIRIS mission dataset. After further analysis these measurements will assist in quantifying the role of thermospheric formed NO_x in the catalytic removal of ozone in the upper stratosphere.

PACS Nos: 33.20.–t, 34.90.+q, 92.60.H–, 92.60.hc, 92.60.hw

Résumé : L'appareil OSIRIS à bord du satellite Odin a détecté le spectre continu dans le visible et l'infrarouge proche produit par la réaction chimioluminescente NO + O → NO_2 + *hν* dans la mésosphère supérieure des régions polaires sombres. Les moyennes journalières du spectre d'émission de NO_2sont obtenues par résolution spectrale du continu NO + O à partir du mélange des fortes bandes de rotation-vibration du OH dans la lueur de haute atmosphère de la mésosphère supérieure. La forme spectrale du continu est alors comparée à des mesures en laboratoire et nous observons un déplacement d'environ 20 nm dans la région de forte pente entre 400 et 800 nm. Nous présentons la forme spectral du continu observé en laboratoire comme référence pour le domaine de 400 à 800 nm. Nous incluons également un exemple du profile en altitude du taux d'émission en volume du continuum de NO_2 obtenu d'un simple balayage en élévation par OSIRIS. Nous observons des radiances de limbe jusqu'à 3×10^9 photons cm^{-2} nm^{-1} s^{-1} au maximum du continuum du NO_2, correspondant à des taux d'émission totale en volume de 2×10^4 photons cm^{-3} s^{-1}. Les données obtenues d'un grand nombre de balayages simples sur une période de 24 h sont rassemblées dans une carte du taux d'émission en volume du continuum de NO_2 dans la région du pôle sud à 90 km d'altitude. La carte illustre les variations spatiales considérables de brillance typiquement observées dans la partie sombre du pôle sud, sur toute la banque de données de OSIRIS. Après une analyse plus poussée, ces mesures nous aiderons à quantifier le rôle du NO_x dans l'appauvrissement de l'ozone de haute atmosphère.

[Traduit par la Rédaction]

1. Introduction

The importance of nitrogen oxides, NO_x = NO + NO_2, in the catalytic destruction of ozone in the stratosphere is summarized by Funke et al. [1] and supported by the Michelson Interferometer for Passive Atmospheric Sounding (MIPAS) measurements of the downward advection of NO_x from the upper mesosphere and lower thermosphere by vortex action in the polar regions. Since NO_x is photochemically stable in the stratosphere it can thus potentially contribute to global ozone variability. Production mechanisms for NO_x in the lower thermosphere have been described by Bailey et al. [2], solar soft X-ray radiance is the dominant source at northern and southern low latitudes and auroral particles are

Received 12 February 2009. Accepted 4 May 2009. Published on the NRC Research Press Web site at cjp.nrc.ca on .

R. Gattinger, D. Degenstein, and E. Llewellyn.[1] ISAS, Department of Physics and Engineering Physics, University of Saskatchewan, Saskatoon, SK S7N 5E2, Canada.
W. Evans. Centre for Research in Earth and Space Sciences (CRESS), York University, 4700 Keele Street, Toronto, ON M3J 1P3, Canada.
I. McDade. Centre for Research in Earth and Space Sciences (CRESS) and Department of Earth and Space Science and Engineering (ESSE); York University, 4700 Keele Street, Toronto, ON M3J 1P3, Canada.

[1]Corresponding author (e-mail: edward.llewellyn@usask.ca).

the driver in the polar regions. Downward advection of NO_x at polar latitudes has also been clearly demonstrated by Randall et al. [3] with measurements made by the Atmospheric Chemistry Experiment Fourier Transform Spectrometer (ACE-FTS) instrument described by Bernath et al. [4].

Mid-latitude rocket-borne observations of the nightglow NO_2 continuum at 540 nm have been analyzed by McDade et al. [5] to infer NO densities in the upper mesosphere and lower thermosphere. Wind Imaging Interferometer (WINDII) observations of the NO_2 continuum at 530 nm were also analyzed by von Savigny et al. [6] to infer mid-latitude NO densities. It is interesting to note that Evans and Shepherd [7] also used the WINDII observations to detect the continuum emission from the NO + O_3 reaction. In the auroral region measurements of the NO_2 continuum at 520 nm a series of rocket flights [8] were used to infer NO densities. Similarly, Witt et al. [9] derived NO densities from a rocket measurement of the continuum at 540 nm under auroral conditions.

For the analysis discussed here, spectra from the Optical Spectrograph and Infra-Red Imager System (OSIRIS) instrument [10] on Odin [11] over the wavelength range 400–800 nm are used to obtain the spectral shape of the NO_2 continuum at 1 km vertical intervals at the tangent limb in the upper mesosphere and lower thermosphere. After removal of the OH night airglow component the observed continuum is compared with laboratory measurements of the NO + O air afterglow made at a series of ambient pressures [12]. The observed laboratory spectral shape at upper mesospheric ambient pressures is presented for reference. Volume emission rates of the NO_2 continuum are derived for a number of limb scans and a Southern Hemisphere polar map of the emission rate at 90 km is presented.

2. Instrumentation and observations

OSIRIS measurements are normally aimed at limb-scattered solar radiation (for example, Gattinger et al. [13]), but in the current study the observations are limited to emissions measured during the Antarctic winter night. The OSIRIS spectral range is from 275 to 810 nm with approximately a 1 nm spectral resolution and with a vertical field of view corresponding to 1 km at the tangent point. The instrument scans the limb at a rate of approximately 0.75 km/s and at mesospheric altitudes the exposure time is nominally 2 s. Absolute limb-pointing knowledge is known to better than 1 km at the tangent point.

Two separate days are chosen for detailed analysis, 18 May 2003 and 26 May 2005, both days frequently exhibiting strong NO_2 continuum emission signals in the south polar region. The general shape of the continuum spectrum is clearly discernable in individual spectra but to improve the signal-to-noise ratio for comparison with laboratory results those spectra with strong continuum emission in the 88 to 100 km region were averaged over approximately ten orbits for each of the two days. The averaged observed limb radiance spectrum for 18 May 2003 is shown in Fig. 1. Spectral signatures present in the spectrum, in addition to the NO_2 continuum and the OH Meinel bands, include the Na doublet at 589 nm, the OI 558 nm atomic line, the $O_2(b^1\Sigma_g^+X^3\Sigma_g^-)$ 0–0 band at 762 nm, and the O_2 Herzberg bands in the 300 nm region. The background signal removed from each limb radiance spectrum is obtained from the OSIRIS uppermost limb scans, typically from 105 to 115 km, and includes both the repeating CCD detector dark pattern and occasional auroral spectral signatures. This dark subtraction process also removes any limb NO_2 continuum signature and thus compromises the spectra over an altitude range of a few kilometres just below the upper altitude limit.

Similarly, an averaged low-latitude (approximately 20° S to 45° S) background OH night airglow spectrum is assembled for each of the two days; the one for 18 May 2003, is shown in Fig. 2. The bright NO_2 continuum produced by auroral particle precipitation is absent in the low-latitude OH background spectra, although a much fainter NO_2 signal, which arises from NO transport from the auroral region plus a contribution from solar soft X-ray irradiation, is expected to be present. Contaminating airglow signals that include the Na, OI, the $O_2(b^1\Sigma_g^+X^3\Sigma_g^-)$ 0–0 band, and the O_2 Herzberg band emissions are also present in the low-latitude spectra. Since this night airglow background spectrum is to be subtracted from the polar spectra, any residual NO_2 continuum present in the background spectrum will result in an underestimate of the NO_2 continuum in the polar regions. However, for the purposes of this study, which is primarily aimed at verifying the NO_2 continuum spectral shape, and as the shape is not expected to change with latitude a slight overcorrection from the airglow component should have no impact on the final conclusions. Nevertheless, a scaled synthetic OH Meinel band spectrum (shown in Fig. 3) is generated to assist in the identification of the very weak OH bands and to establish more precisely the residual NO_2 continuum level present in the observed airglow spectrum shown in Fig. 2. The assumed OH vibrational level relative populations are from McDade and Llewellyn [14] and the relative transition probabilities are from Murphy [15] and Turnbull and Lowe [16]. The relative Meinel band intensities are in general agreement with the night airglow observations of Broadfoot and Kendall [17]. After correcting for the weak OH Meinel bands present in the 550 to 600 nm region in Fig. 2, it is estimated that the residual continuum in Fig. 2 is less than 5×10^7 photons cm^{-2} nm^{-1} s^{-1} in the 570 nm region, the approximate location of the peak of the NO_2 continuum shape. This estimate is based on the differential brightness derived from Fig. 3. By comparison the observed 570 nm signal in Fig. 1 is approximately 1×10^9 photons cm^{-2} nm^{-1} s^{-1}, a factor of 20 larger than the residual NO_2 signal in the background spectrum. Thus, any future analyses aimed at determining the absolute brightness of the NO_2 continuum could be in error by approximately 5% and so influence products derived using the measured NO_2 absolute brightness.

When the averaged low-latitude limb radiance night airglow spectrum (Fig. 2), which is dominated by the OH Meinel bands, is subtracted from the averaged total limb radiance spectrum (Fig. 1) the difference spectrum shown in Fig. 4 results. As expected, the removal of the OI 558 nm emission line, and the $O_2(b^1\Sigma_g^+X^3\Sigma_g^-)$ 0–0 band at 762 nm, is not exact, but the removal of the OH band signatures is sufficiently accurate to show the residual NO_2 continuum spectrum. A similar plot of the difference spectrum of the two averaged OSIRIS limb radiance spectra for the second day of this analysis (26 May 2005) is shown in Fig. 5. The two corresponding averaged limb radiance spectra are very

Fig. 1. The averaged OSIRIS limb radiance spectrum for 18 May 2003, Antractic night conditions with bright continuum emission. The data gap in the 500 nm region is the result of the order sorter included in the OSIRIS spectrograph design. The continuum beginning long wave of 400 nm is produced by the NO + O → NO_2 + *hν* chemiluminescent reaction occurring in the upper mesosphere and lower thermosphere. Additional features include the OH Meinel vibration–rotation bands that occur in the night airglow, the 762 nm $O_2(b^1\Sigma_g^+X^3\Sigma_g^-)$ 0–0 band (offscale), the OI 558 nm emission (offscale), the Na doublet at 589 nm, and the Herzberg bands in the 300 nm region.

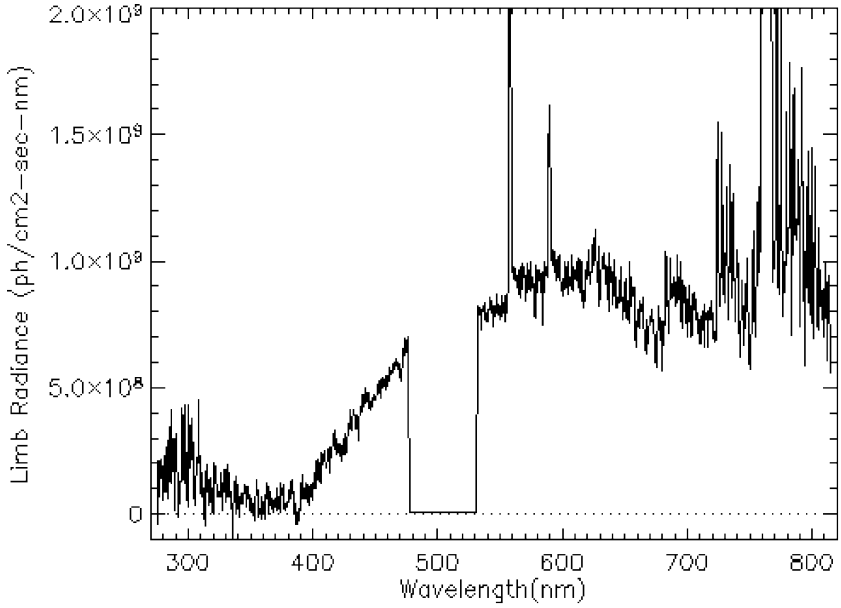

Fig. 2. The averaged OSIRIS low-latitude night airglow background spectrum for 18 May 2003, latitude range approximately 20° S to 45° S; observations exclude the effects of auroral particle generation of the NO_2 continuum. The OH 690 nm 7–2, 730 nm 8–3, 775 nm 9–4, and 790 nm 5–1 bands are all clearly visible in the spectrum. The 762 nm $O_2(b^1\Sigma_g^+X^3\Sigma_g^-)$ 0–0 band (offscale), the OI 558 nm emission (offscale), the 589 nm Na doublet, and the Herzberg bands in the 300 nm region are also present.

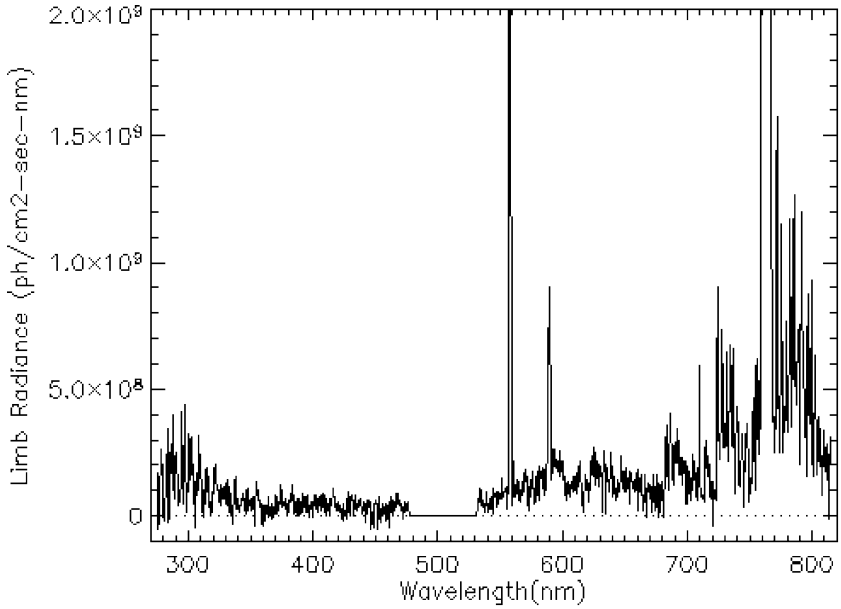

similar to those shown in Figs. 1 and 2. The repeatability of the NO_2 continuum signature using data from the two separate days is apparent. The NO_2 continuum emission for 26 May 2005, is slightly weaker than for 18 May 2003. As in Fig. 4 the OH Meinel bands are almost completely absent, the OI 558 nm feature is slightly over-corrected, the 589 nm Na doublet is present and the 762 nm $O_2(b^1\Sigma_g^+X^3\Sigma_g^-)$ 0–0 band is again bright.

3. Comparison with laboratory spectrum

The spectral shape of the NO + O → NO_2 + *hν* chemiluminescent reaction rate has been measured by Becker et al. [12] for a series of ambient pressures. The 1 mTorr pressure curve, which is applicable to the mesopause region, was selected for comparison with the OSIRIS results. The measured laboratory spectrum, scaled for comparison purposes to

Fig. 3. A scaled synthetic OH spectrum in the 500 to 810 nm region to identify the weak OH Meinel bands present in the observed night airglow background spectrum shown in Fig. 2. The synthetic spectrum is convolved with the OSIRIS 1 nm slit width. Additional bands identifiable in the observed spectrum are 8–2 at 590 nm and 9–3 at 625 nm.

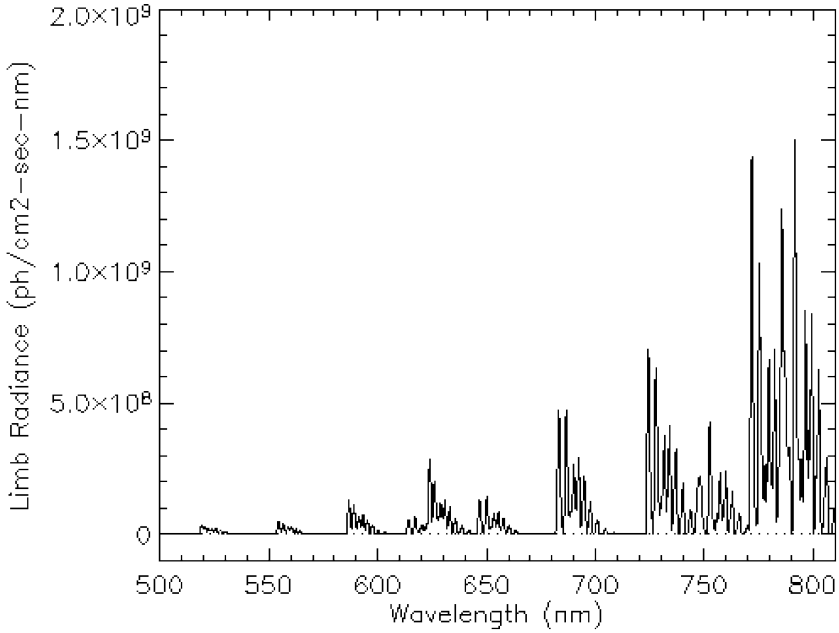

Fig. 4. The difference of the two averaged OSIRIS limb radiance spectra for 18 May 2003, (Fig. 1 spectrum minus Fig. 2 spectrum). The square symbols are the measured NO_2 continuum from the Becker et al. [12] laboratory spectra for a pressure of 1 mTorr (1 Torr = 133.3 pa), scaled to the observed OSIRIS NO_2 continuum curve at 580 nm.

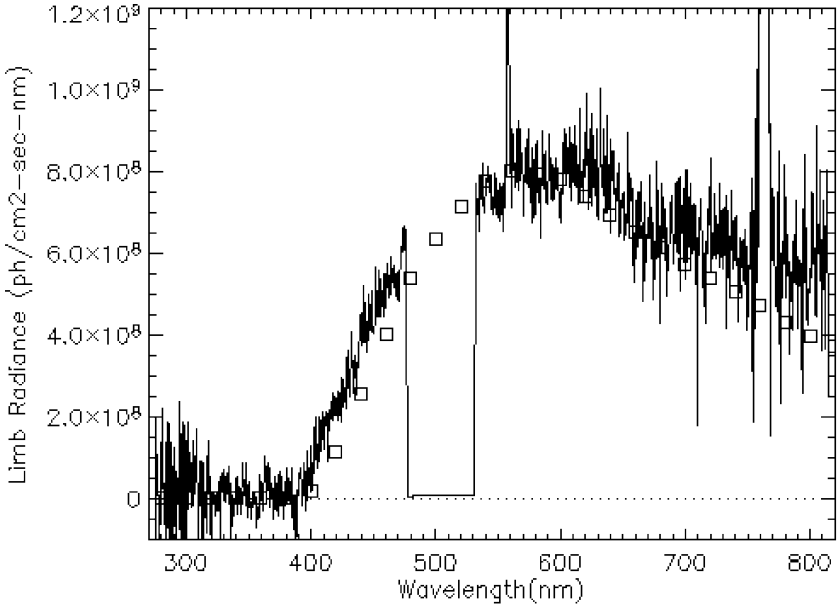

match the OSIRIS observed NO_2 continuum curve, is indicated by the square symbols in Figs. 4 and 5. There appears to be a small, but significant, difference for both days between the OSIRIS measurements and the laboratory results on the short-wave side of the peak – the observed spectral shape from the OSIRIS measurements is shifted approximately 20 nm towards shorter wavelengths in the steeply sloped 400 to 500 nm region as compared with the laboratory results. The reliability of the comparison long wave of the peak is more difficult to assess due to the uncertainty in the OH Meinel band subtraction procedure.

Since the spectral shape of the NO_2 continuum observed by OSIRIS differs noticeably from the measured laboratory spectrum (Figs. 4 and 5) a revised continuum spectral shape is included in Table 1. This spectral shape, which covers the range 400 to 800 nm, is determined from the observed OSIRIS averaged spectra. From the spectrally complete continuum shape determined by Becker et al. [12] the equivalent

Fig. 5. The same as for Fig. 4 but for 26 May 2005. Again the square symbols are from the Becker et al. [12] laboratory spectra for a pressure of 1 mTorr, scaled to the observed OSIRIS NO_2 continuum curve at 580 nm.

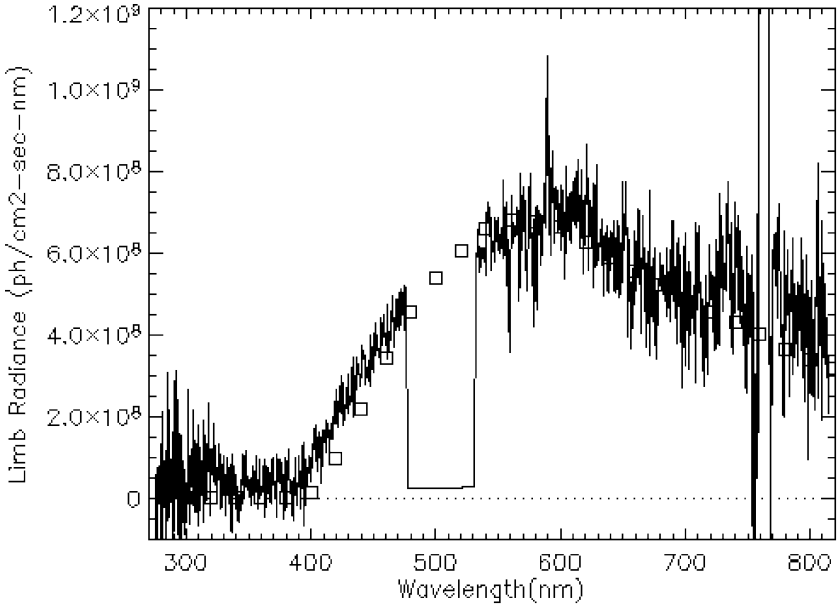

Table 1. Normalized spectrum of NO + O → NO_2 + *hv* chemiluminescent reaction rate measured by OSIRIS. Numbers in brackets near 500 nm are interpolated over the spectral order sorter region.

Wavelength (nm)	Normalized rate	Wavelength (nm)	Normalized rate	Wavelength (nm)	Normalized rate
360	0.00	520	(0.88)	680	0.79
380	0.01	540	0.94	700	0.74
400	0.10	560	0.98	720	0.70
420	0.26	580	1.00	740	0.65
440	0.44	600	0.99	760	0.61
460	0.63	620	0.96	780	0.56
480	0.75	640	0.90	800	0.51
500	(0.82)	660	0.85	820	0.49

width of the total NO_2 continuum, extending from 400 nm to 1400 nm, is found to be approximately 450 nm with a peak at 580 nm for low-pressure conditions. The revised values in Table 1 from the OSIRIS results are normalized to unity at the observed continuum peak, 580 nm, to simplify the conversion from differential brightness measured at any location within the continuum to the integrated continuum brightness using the 450 nm equivalent width. In this way, measured photon emission rates can be converted to species density products using known chemical reaction rates. For the NO + O bimolecular reaction, an integrated rate of 4.2×10^{-18} cm^3 mol^{-1} s^{-1} is given by Becker et al. [12]. For the termolecular reaction Whytock et al. [18] determined a rate of 15.5×10^{-33} exp(1160/1.987T) cm^6 mol^{-2} s^{-1}. The revised continuum shape listed in Table 1 is used to determine the spectrally integrated NO_2 volume emission rates presented in the next section.

4. Application to OSIRIS data

Limb radiance altitude profiles of the NO_2 continuum are derived for each limb scan and then inverted to obtain volume emission-rate altitude profiles. The radiance profiles are obtained by first removing the repeating CCD dark pattern using the spectra observed at the upper limit of each limb scan, then interpolating to a 1 km altitude grid, and then solving with a simultaneous least-squares spectral fit at each altitude for a scaled averaged OH spectrum (Fig. 2) and a scaled NO_2 continuum spectrum (Table 1). An example of this fitting procedure is shown in Fig. 6*a* for two altitudes. It should be noted again that these are individual spectra. The noise level in the "Limb Observed" spectrum is not smoothed and spurious noise spikes are not removed. Although there is considerable noise in each limb spectrum compared to the NO_2 continuum signal, establishing a spectral fit to the whole continuum region considerably enhances the final signal-to-noise ratio in the determination of the NO_2 component in the limb radiance at each 1 km altitude interval. Spectral intervals that include known contaminating sources, for example, 558 nm OI, 762 nm $O_2(b^1\Sigma_g^+X^3\Sigma_g^-)$ 0–0 band, and 589 nm Na, are excluded from the fitting procedure. These contaminating features, which commonly occur in the night airglow and (or) in the aurora, each exhibit an altitude profile that differs from the NO_2 continuum altitude profile and must be ex-

Fig. 6. (*a*) Examples of limb radiance spectra at two altitudes together with the combined least-squares fitting of the scaled low-latitude OSIRIS background OH spectrum and scaled NO_2 continuum spectrum from Table 1. The individual spectra are a subset of the limb scan spectra obtained on 26 May 2005, 15:10 UT, latitude 82°S, longitude 123°E, solar zenith angle 119°, solar local time 23:25. The difference spectrum has been smoothed to improve clarity. (*b*) An NO_2 continuum volume emission-rate altitude profile from a single OSIRIS limb scan, 26 May 2005, 15:10 UT, latitude 82°S, longitude 123°E, solar zenith angle 119°, solar local time 23:25, as in Fig. 6*a*. The volume emission rate is based on the total NO_2 continuum from 400 to 1400 nm assuming a spectral shape equivalent width of 450 nm (see text). The volume emission rate errors at each altitude are derived from the noise-induced continuum uncertainty in the limb radiance measurements. The noise level seen in Fig. 6*a* is typical.

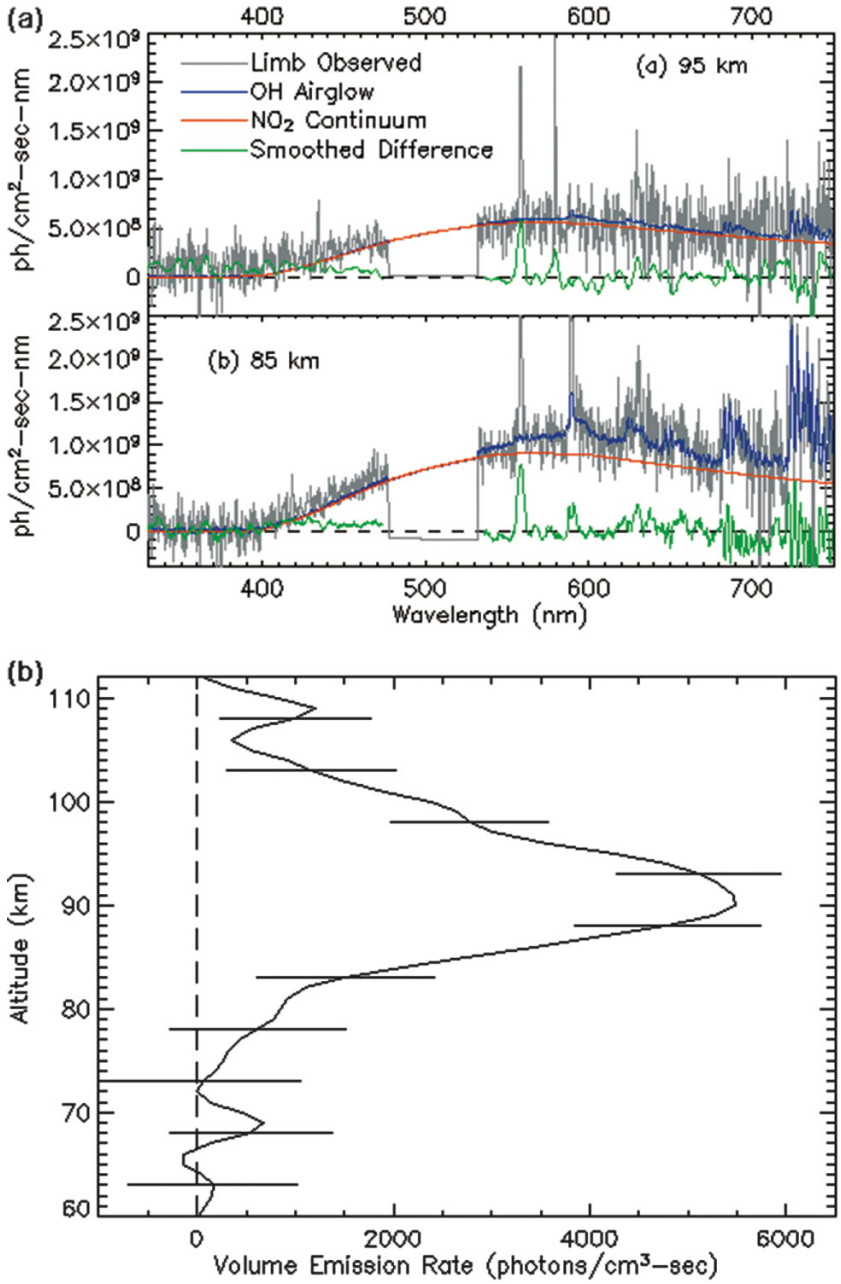

cluded. The "Smoothed Difference" spectrum is the smoothed difference between the Limb Observed spectrum and the sum of the scaled OH and NO_2 continuum spectra. As expected the OH component at 95 km is much fainter than at 85 km. Peak NO_2 continuum limb radiances in excess of 3×10^9 photons cm^{-2} nm^{-1} s^{-1} are observed on occasion.

A simple iterative "onion-peel" procedure is used to invert the derived NO_2 limb radiance altitude profiles to obtain volume emission-rate altitude profiles. The inversion procedure assumes emission spherical symmetry in concentric 1 km layers and derives the volume emission rate in each layer based on the layer path lengths along the line of sight; this procedure is started at the uppermost layers where the emission rate is typically below the detection limit of OSIRIS. An example of a derived OSIRIS NO_2 volume emission rate altitude profile is shown in Fig. 6*b*; this is for

Fig. 7. NO_2 volume emission rate map (photons cm^{-3} s^{-1}) for the Antarctic region, 26–27 May 2005, minimum solar zenith angle 101°, horizontal slice at 90 km altitude, extracted from 164 OSIRIS altitude profiles of the type shown in Fig. 6*b*. Squares indicate the location of each OSIRIS limb scan. The data gap within 8° of the South Pole is due to the Odin orbit. The interpolation is with an inverse second order nearest-neighbour weighting.

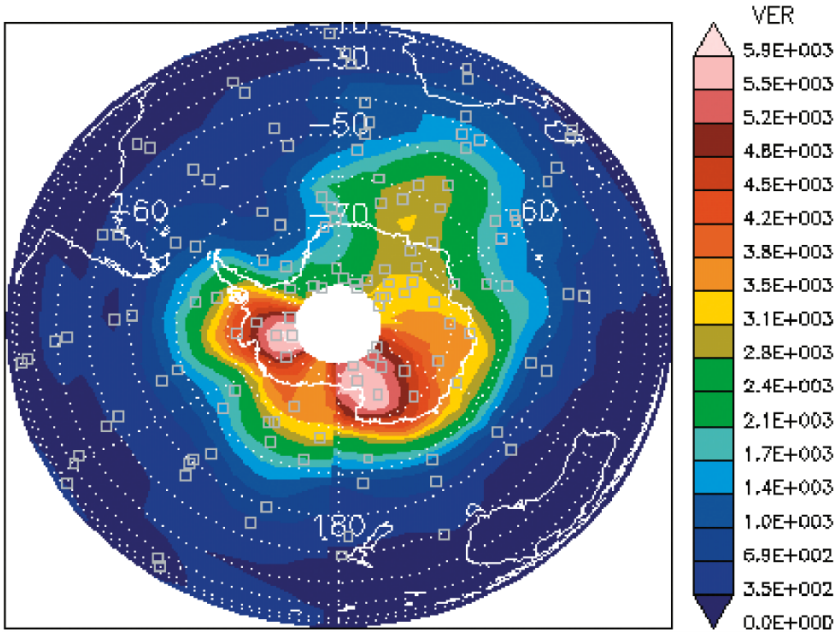

the same limb scan as in Fig. 6*a*. The limb scan upper limit in this case is 114 km and thus provides useful data to above 110 km. Peak NO_2 continuum volume emission rates in excess of 2×10^4 photons cm^{-3} s^{-1} are observed on occasion.

As a simple check on the validity of the OSIRIS NO_2 observations comparisons are made here with previous observations. Two high-latitude observations are relevant, one by Witt et al. [9] and one by Sharp [8]. From their results an average vertically integrated differential brightness of approximately 1.6×10^7 photons cm^{-2} s^{-1} nm^{-1} is obtained. This corresponds to a total NO_2 continuum of approximately 8×10^9 photons cm^{-2} s^{-1} for an assumed equivalent width of 450 nm and a normalization scaling factor of 0.9, Table 1, for measurments made at approximately 520 nm rather than at the continuum peak at 580 nm. From Fig. 6*b* the vertically integrated brightness observed by OSIRIS is approximately 7×10^9 photons cm^{-2} s^{-1}, in good agreement with the earlier results.

The OSIRIS NO_2 continuum observations indicate a pronounced longitudinal variability in the polar regions. The Southern Hemisphere polar map in Fig. 7 shows the NO_2 volume emission rate at 90 km altitude derived from OSIRIS data for 26–27 May 2005. Longitudinal brightness variation at 75° S latitude is approximately a factor of four. The latitudinal distribution shown in Fig. 7 hints at the potential for tracking the equatorward drift of NO_x. The OSIRIS NO_2 volume emission rate data used to compile the polar map in Fig. 7 are taken from the completed Odin mission analysis suite.

As the OSIRIS spectra also include the 762 nm O_2 ($b^1\Sigma_g^+ X^3\Sigma_g^-$) 0–0 band it is possible to derive the [O] altitude profile in the Antarctic polar night. Thus, using the NO + O → NO_2 + *hv* reaction, together with a knowledge of the spatial distribution in the dark polar regions of both the NO_2 continuum and the [O] altitude profile, will allow the determination of the [NO] distribution. Future OSIRIS studies will be directed towards determining the [O] and the [NO] spatial distributions in the dark polar night for the complete OSIRIS mission; ultimately this will be added to the broader NO_x database. However, it must be stressed that the NO_2 observations only yield information on the NO_2 formation rate and not the local NO_2 concentration. These OSIRIS indirect [NO] measurements will potentially be supplemented by independent direct [NO] observations using stellar occultation in the dark polar regions, as proposed by Lumpe et al. [19].

5. Conclusions

The visible and near infrared continuum spectrum produced by the NO + O → NO_2 + *hv* chemiluminescent reaction has been detected in the upper mesospheric and lower thermospheric dark polar regions by OSIRIS on the Odin spacecraft. After removal of the blended bright upper mesospheric OH vibration–rotation airglow band emissions, the observed continuum spectral shape is compared with the continuum spectrum measured in the laboratory by Becker et al. [12]. The spectral shape observed by OSIRIS is shifted to lower wavelengths by approximately 20 nm in the steeply sloped 400 to 500 nm region. A normalized spectral shape of the NO_2 continuum observed by OSIRIS over the 400 to 800 nm range is provided for reference.

Limb radiance altitude profiles of the NO_2 continuum are derived and inverted to yield volume emission-rate altitude profiles. The observed limb radiances of up to 3×10^9 photons cm^{-2} nm^{-1} s^{-1}, at the peak of the NO_2 continuum, correspond to volume emission rates of approximately 2×10^4 photons cm^{-3} s^{-1}. These results are in agreement with independent earlier measurements in the auroral zone.

The spatial sampling frequency of the OSIRIS limb scan locations is sufficient to produce polar maps of the three-dimensional distribution of the NO_2 continuum in the dark polar regions. A sample map shows the pronounced longitudinal variation that is typically observed. Also, the observed latitudinal distribution hints at the potential for tracking the equatorward drift of NO_x species.

The presented set of OSIRIS measurements offers a valuable extension to the existing suite of NO_x observations in the upper mesosphere and lower thermosphere. However, it is important to establish the rate of downward advection of NO_x species in the polar vortices to enable quantitative assessment of subsequent catalytic removal of ozone in the upper stratosphere.

Further analysis of the OSIRIS data set is planned, this will derive NO densities in the dark polar regions for the entire mission The planned analysis will include a concurrent determination of the atomic oxygen density in the region of the mesopause using the 762 nm $O_2(b^1\Sigma_g^+X^3\Sigma_g^-)$ 0–0 band, which is also observed by OSIRIS.

Acknowledgements

This work was supported by the Canadian Space Agency and the Natural Sciences and Engineering Research Council (Canada). Odin is a Swedish-led satellite project funded jointly by Sweden (SNSB), Canada (CSA), France (CNES), and Finland (Tekes).

References

1. B. Funke, M. López-Puertas, S. Gil-López, T. von Clarmann, G.P. Stiller, H. Fischer, and S. Kellmann. J. Geophys. Res. **110**, D24, D24308 (2005). doi:10.1029/2005JD006463.
2. S.M. Bailey, C.A. Barth, and S.C. Solomon. J. Geophys. Res. **107**, A8, 1205 (2002). doi:10.1029/2001JA000258.
3. C.E. Randall, V.I. Harvey, C.S. Singleton, P.F. Bernath, C.D. Boone, and J.U. Kozyra. Geophys. Res. Lett. **33**, L18811 (2006). doi:10.1029/2006GL027160.
4. P.F. Bernath, C.T. McElroy, M.C. Abrams, C.D. Boone, M. Butler, C. Camy-Peyret, M. Carleer, C. Clerbaux, P.-F. Coheur, R. Colin, P. DeCola, M. De Mazière, J.R. Drummond, D. Dufour, W.F.J. Evans, H. Fast, D. Fussen, K. Gilbert, D.E. Jennings, E.J. Llewellyn, R.P. Lowe, E. Mahieu, J.C. McConnell, I.C. McDade, M. McHugh, S.D. McLeod, D. Michelangeli, C. Midwinter, R. Nassar, F. Nichitiu, C.P. Rinsland, Y.J. Rochon, P. Simon, R. Skelton, J.J. Sloan, M.-A. Soucy, K. Strong, P. Tremblay, D. Turnbull, K.A. Walker, I. Walkty, D.A. Wardle, V. Wehrle, R. Zander, and J. Zou. Geophys. Res. Lett. **32**, L15S01 (2005). doi:10.1029/2005GL022386.
5. I.C. McDade, E.J. Llewellyn, R.G.H. Greer, and D.P. Murtagh. Planet. Space Sci. **34**, 801 (1986). doi:10.1016/0032-0633(86)90076-0.
6. C.H. von Savigny, I.C. McDade, G.G. Shepherd, and Y. Rochon. Ann. Geophys. **17**, 1439 (1999). doi:10.1007/s005850050868.
7. W.F.J. Evans and G.G. Shepherd. Geophys. Res. Lett. **23**, 3623 (1996). doi:10.1029/96GL03333.
8. W.E. Sharp. J. Geophys. Res. **83**, A9, 4373 (1978). doi:10.1029/JA083iA09p04373.
9. G. Witt, J. Rose, and E.J. Llewellyn. J. Geophys. Res. **86**, A2, 623 (1981). doi:10.1029/JA086iA02p00623.
10. E.J. Llewellyn, N.D. Lloyd, D.A. Degenstein, R.L. Gattinger, S.V. Petelina, A.E. Bourassa, J.T. Wiensz, E.V. Ivanov, I.C. McDade, B.H. Solheim, J.C. McConnell, C.S. Haley, C. von Savigny, C.E. Sioris, C.A. McLinden, E. Griffioen, J. Kaminski, W.F.J. Evans, E. Puckrin, K. Strong, V. Wehrle, R.H. Hum, D.J.W. Kendall, J. Matsushita, D.P. Murtagh, S. Brohede, J. Stegman, G. Witt, G. Barnes, W.F. Payne, L. Piché, K. Smith, G. Warshaw, D.-L. Deslauniers, P. Marchand, E.H. Richardson, R.A. King, I. Wevers, W. McCreath, E. Kyrölä, L. Oikarinen, G.W. Leppelmeier, H. Auvinen, G. Mégie, A. Hauchecorne, F. Lefèvre, J. de La Nöe, P. Ricaud, U. Frisk, F. Sjoberg, F. von Schéele, and L. Nordh. Can. J. Phys. **82**, 411 (2004). doi:10.1139/p04-005.
11. D.P. Murtagh, U. Frisk, F. Merino, M. Ridal, A. Jonsson, J. Stegman, G. Witt, P. Eriksson, C. Jiménez, G. Megie, J. de la Nöe, P. Ricaud, P. Baron, J.R. Pardo, A. Hauchcorne, E.J. Llewellyn, D.A. Degenstein, R.L. Gattinger, N.D. Lloyd, W.F.J. Evans, I.C. McDade, C.S. Haley, C. Sioris, C. von Savigny, B.H. Solheim, J.C. McConnell, K. Strong, E.H. Richardson, G.W. Leppelmeier, E. Kyrölä, H. Auvinen, and L. Oikarinen. Can. J. Phys. **80**, 309 (2002). doi:10.1139/p01-157.
12. K.H. Becker, W. Groth, and D. Thran. Chem. Phys. Lett. **15**, 215 (1972). doi:10.1016/0009-2614(72)80152-0.
13. R.L. Gattinger, D.A. Degenstein, and E.J. Llewellyn. J. Geophys. Res. **111**, D13, D13303 (2006). doi:10.1029/2005JD006369.
14. I.C. McDade and E.J. Llewellyn. Ann. Geophys. **11**, 47 (1993).
15. R.E. Murphy. J. Chem. Phys. **54**, 4852 (1971). doi:10.1063/1.1674762.
16. D.N. Turnbull and R.P. Lowe. Planet. Space Sci. **37**, 723 (1989). doi:10.1016/0032-0633(89)90042-1.
17. A.L. Broadfoot and K.R. Kendall. J. Geophys. Res. **73**, 426 (1968). doi:10.1029/JA073i001p00426.
18. D.A. Whytock, J.V. Michael, and W.A. Payne. Chem. Phys. Lett. **42**, 466 (1976). doi:10.1016/0009-2614(76)80655-0.
19. J.D. Lumpe, S. Bailey, B. McClintock, and C. Randall. Observing nitric oxide in the polar night by stellar occultation, Eos Trans. AGU, Fall Meeting Suppl., Abstract #SA23A–1128. 2007.